Product review

Paleomagnetism.org: An online multi-platform open source environment for paleomagnetic data analysis

Mathijs R. Koymans [*,1], Cor G. Langereis, Daniel Pastor-Galán, Douwe J.J. van Hinsbergen

Department of Earth Sciences, University of Utrecht, Budapestlaan 4, 3584 CD Utrecht, The Netherlands

ARTICLE INFO

ABSTRACT

This contribution provides an overview of Paleomagnetism.org, an open-source, multi-platform online environment for paleomagnetic data analysis. Paleomagnetism.org provides an interactive environment where paleomagnetic data can be interpreted, evaluated, visualized, and exported. The Paleomagnetism.org application is split in to an interpretation portal, a statistics portal, and a portal for miscellaneous paleomagnetic tools.

In the interpretation portal, principle component analysis can be performed on visualized demagnetization diagrams. Interpreted directions and great circles can be combined to find great circle solutions. These directions can be used in the statistics portal, or exported as data and figures.

The tools in the statistics portal cover standard Fisher statistics for directions and VGPs, including other statistical parameters used as reliability criteria. Other available tools include an eigenvector approach foldtest, two reversal test including a Monte Carlo simulation on mean directions, and a coordinate bootstrap on the original data. An implementation is included for the detection and correction of inclination shallowing in sediments following TK03.GAD. Finally we provide a module to visualize VGPs and expected paleolatitudes, declinations, and inclinations relative to widely used global apparent polar wander path models in coordinates of major continent-bearing plates.

The tools in the miscellaneous portal include a net tectonic rotation (NTR) analysis to restore a body to its paleo-vertical and a bootstrapped oroclinal test using linear regressive techniques, including a modified foldtest around a vertical axis.

Paleomagnetism.org provides an integrated approach for researchers to work with visualized (e.g. hemisphere projections, Zijderveld diagrams) paleomagnetic data. The application constructs a custom exportable file that can be shared freely and included in public databases. This exported file contains all data and can later be imported to the application by other researchers. The accessibility and simplicity through which paleomagnetic data can be interpreted, analyzed, visualized, and shared makes Paleomagnetism.org of interest to the community.

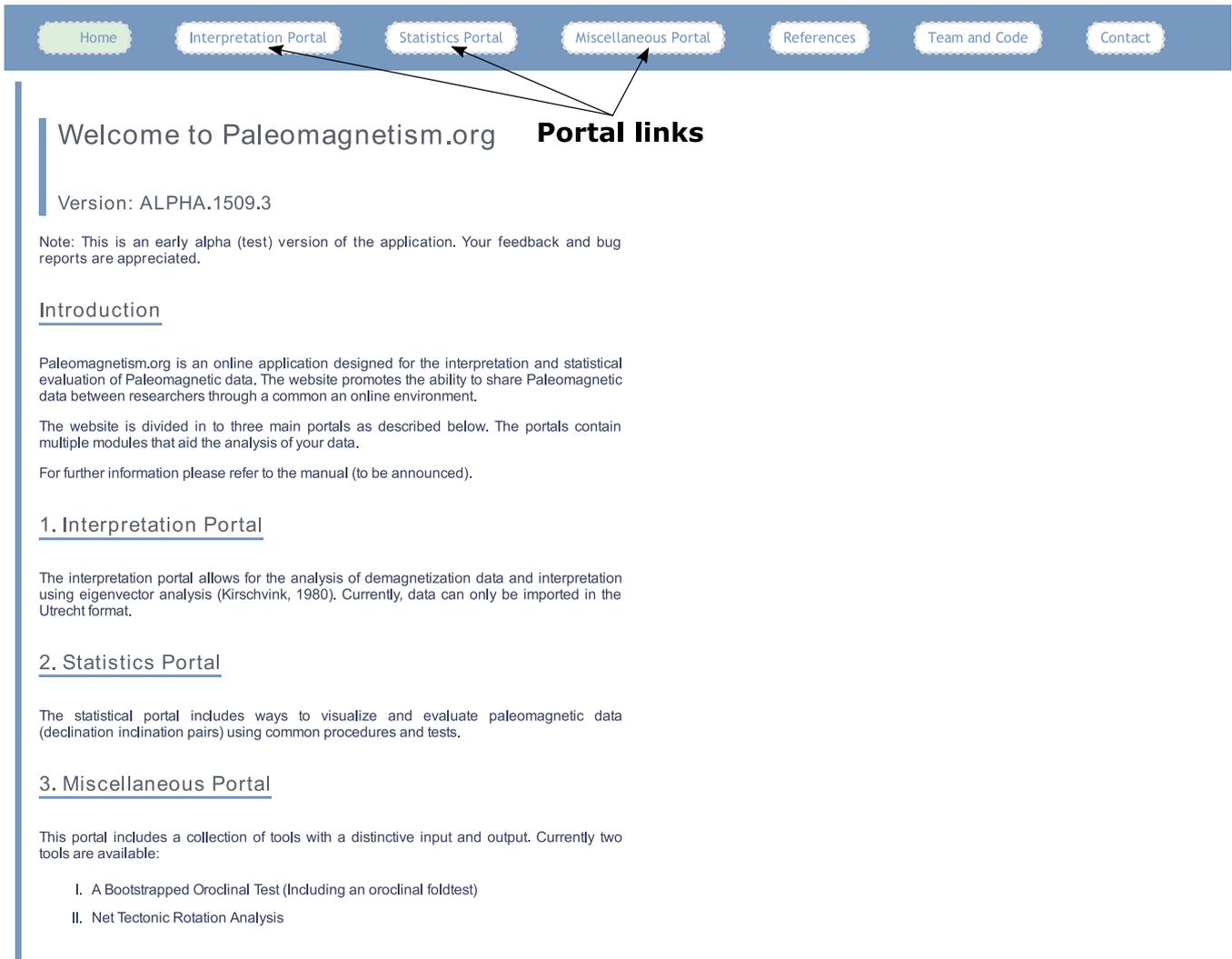© 2016 Elsevier Ltd. All rights reserved.

1. Introduction

Paleomagnetic data provide quantitative information on the paleolatitude and vertical axis rotation of rocks and are instrumental for paleogeographic and tectonic reconstuctions. In particular, the behavior of the magnetic field known as paleo-secular variation, but also measurement uncertainties, induce scatter in paleomagnetic data (e.g., Butler, 1992; Johnson et al., 2008, Biggin et al., 2008, Tauxe et al., 2010, Deenen et al., 2011). Accurate statistical treatments of these data are therefore fundamental in paleomagnetism. In the paleomagnetic community it is common practice to publish means of magnetic directions with a few standard statistical parameters. In many cases, the original data remain unavailable to the reader and are rarely included in public databases (e.g. MagIC, http://earthref.org/MagIC). We provide an accessible and intuitive online platform (Fig. 1) to interpret demagnetization data, perform standard statistical treatments, plot paleomagnetic data, and compare them against apparent polar wander paths. This software contribution builds upon, and is inspired by other software packages including PALDIR, Remasoft, PaleoMac, and the PmagPy library (Tauxe et al., 2016; https://earthref.org/PmagPy/cookbook/). The data used in our application can be exported to simple data files and shared freely with the community and included in public databases at will. This contribution serves as a manual for the use of, and describes the scientific background behind the current portals and modules on Paleomagnetism.org. Since we provide an open source

* Corresponding author.
  E-mail address: koymans@knmi.nl (M.R. Koymans).
  [1] Current address: Paleomagnetic Lab Fort Hoofddijk, Utrecht University, Budapestlaan 17, 3584 CD Utrecht, The Netherlands.

Fig. 1. Homepage – Screenshot of the home page of Paleomagnetism.org. The three available portals can be used by clicking the respective menu links at the top of the page.

environment, it is foreseen that useful additions will appear in time.

In the interpretation portal, principle component analysis (Kirschvink, 1980) can be applied to fit great circles and directional set-points on demagnetization data visualized on Zijderveld diagrams (Zijderveld, 1967), equal area projections, and intensity decay diagrams. Great circle solutions can be found with or without independent set-points using the iterative procedure of McFadden and McElhinny (1988). Interpreted directions can be exported as a tabulated *.csv* file or as a custom *.dir* file that contains all data and interpretations made by the user. Interpreted magnetic directions can also be forwarded and imported to the statistics portal for further statistical analysis.

The statistics portal provides modules containing common paleomagnetic tests for the statistical analysis on both directional and VGP distributions. These tests are contained within separate modules and include reversal, or common true mean direction tests (McFadden and McElhinny, 1990; Tauxe et al., 2010), the eigenvector approach fold test (Tauxe and Watson, 1994), a tool for the correction of inclination shallowing in sediments after the TK03.GAD field model (Tauxe and Kent, 2004; Tauxe et al., 2008), and a module to compare results with common apparent polar wander paths in the coordinates of the most important continent-bearing plates. For all data that is added to the application, a cutoff (none, Vandamme, or 45°) can be applied (Vandamme, 1994; Johnson et al., 2008) to the VGP distribution. Standard Fisher parameters (Fisher, 1953) are calculated and the data can be used in the other application modules. Data added to the statistics

portal can be exported to the custom *.pmag* file format.

In the miscellaneous portal we provide a module for a net tectonic rotation analysis (NTR) that can be used to restore a body to its paleo-vertical. In the oroclinal module, a bootstrapped linear total least squares regression can be performed on bi-dimensional data as an oroclinal test, in addition to an oroclinal foldtest around a vertical-axis based on circular statistics and other helpful statistical tools.

Data for a single session is stored within the browsers dedicated local storage. Data can be cleared from memory in the advanced option tabs in the portal. Before resetting the instance, we recommend exporting the data and saving your instance locally. Analysis of the exported instance can be continued at any time by importing the previously exported saved file (*.pmag* and *.dir*). These files can also be added as supplementary information to publications for full data and analytical disclosure, and uploaded into common public databases (e.g. MagIC).

2. Interpretation portal

In the introductory tab of the interpretation portal users can import demagnetization data from existing plain-text formats (currently supporting the Utrecht, Munich, PGL Beijing, and PaleoMac format). Support for more formats will be added in the future through collaboration with users and we emphasize the open-source nature of the application.

2.1. Interpretation module

In the interpretation module (Fig. A1), the keyboard can be used to navigate through the interpretation portal using the keys specified on the portal's screen. Equal area projections and Zijderveld diagrams (Fig. 2), intensity decay, vector difference sum, and unblocking spectrums are illustrated for each specimen and can be interacted with in multiple coordinate reference frames, given that core and bedding orientations are specified for each sample. Directions and great circles can be fitted to the demagnetization data following the eigenvector principle component analysis described by (Kirschvink 1980), and can optionally be anchored to the origin. Any interpretation made is automatically completed in geographic coordinates and tectonic coordinates, provided the bedding orientation for each specimen is specified.

2.2. Fitting module

The fitting module (Fig. A2) illustrates all interpreted components and great circles on an equal area projection. With a combined set of interpreted directional set-points and great circles, best-fit great circle solutions can be determined using the directional data as independent set-points following the iterative algorithm described by (McFadden and McElhinny, 1988). If no set-points are available (i.e. the set of interpretations only constitutes great circles), a closest clustering of directions on these great circles is interpreted, whereby only the polarity of the magnetic directions will be prompted to the user. In this module, directions can be saved to the statistics portal to be used there or exported as tabulated data.

2.3. Interpretation portal: advanced options

In the advanced options tab (Fig. A3), tabulated data can be saved to tabulated .csv files or exported and imported to and from the custom *.dir* format. This file can be shared with other researchers giving full visual disclosure of the original data and interpretation made by the user. Other options include adding a sticky direction to the equal area projections (e.g. present day magnetic north), showing demagnetization step labels, normalizing intensities, or including the origin as a demagnetization point during the PCA. The application can be reset and all locally stored information will be cleared from the browser.

3. Statistical modules

The statistics portal is divided in multiple modules. A short description of the procedures, scientific background, and philosophy are given below. In the introductory tab, magnetic directions can be added to the application. The data input (Fig. A4) for the statistics portal requires declination-inclination pairs with optionally included bedding orientations and a sample code. Alternatively, the data input window allows previously saved magnetic directions to be imported directly from the interpretation portal. The application allows for the random sampling of
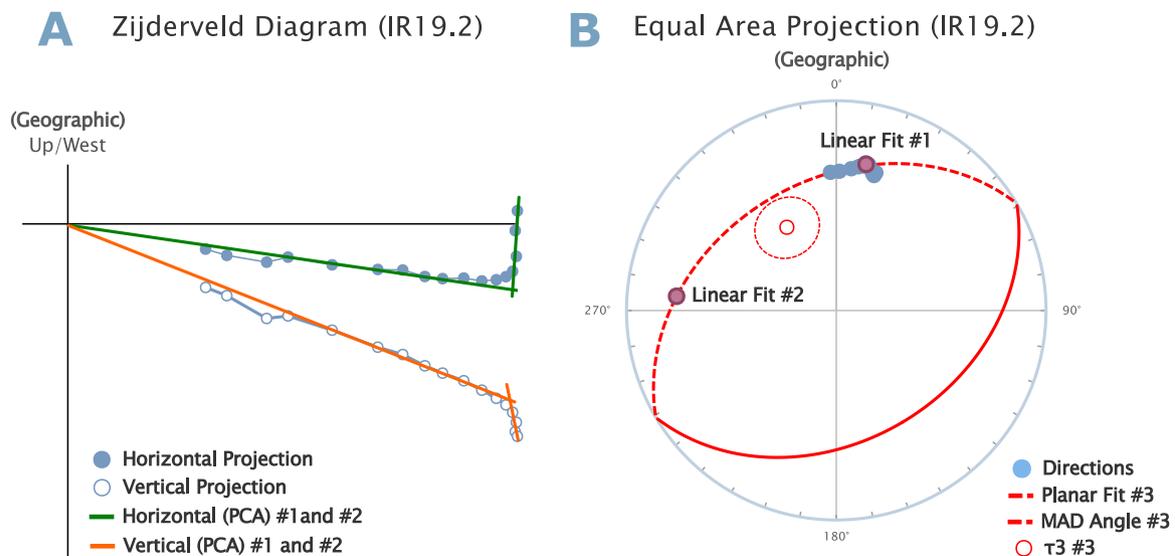

Fig. 2. Interpretation Portal – (a) Zijderveld diagram illustrating a multi-component thermal demagnetization diagram with two interpreted components. (b) Equal area projection of the same data, including a fitted great circle through both components. All interpreted directions and great circles are numbered on the equal area projection as "linear fit" and "planar fit" respectively.

A CHRM Directions
CS – M–L Jur

B Relative VGP Positions
CS – M–L Jur

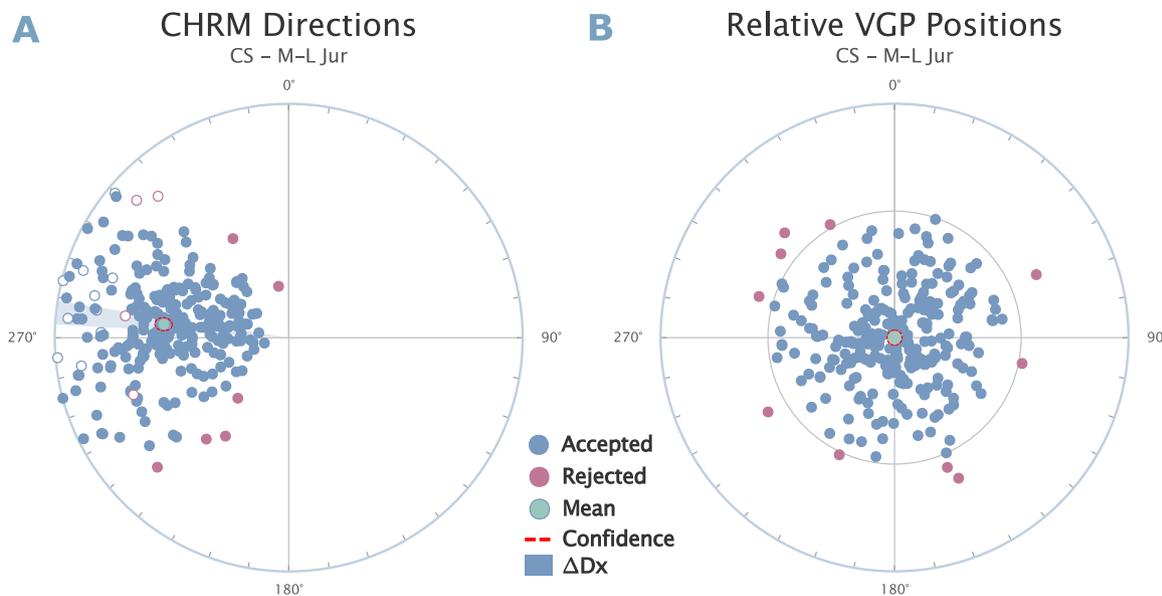- Accepted
- Rejected
- Mean
- -- Confidence
- ΔDx

Fig. 3. Geomagnetic Direction Module – equal area projections of Cretaceous data showing (a) ChRM directions of points accepted (blue) and rejected (red) after a 45-cutoff has been applied, including a mean direction and confidence ellipse. (b) Relative VGP positions with the mean VGP rotated to North. The illustrated confidence envelopes are based on the A95 parameter for the VGP distribution (see Deenen et al., 2011). (For interpretation of the references to color in this figure legend, the reader is referred to the web version of this article.)

Fisherian distributions (N, κ) of directions or VGPs for a given mean direction. Site meta-data (e.g. age and age uncertainties, location coordinates, and author) can be added under the advanced options field. Each added set of directions is defined as a site, and represents a location with a single latitude and longitude. An unlimited number of sites can be added to the application.

3.1. Geomagnetic directions module

It has long been recognized (e.g. Creer, 1962; Cox, 1970) and later re-emphasized (e.g. Tauxe et al., 2008, Tauxe et al., 2010; Deenen et al., 2011) that the scatter of directional data induced by paleo-secular variation becomes increasingly N–S elongated with lower latitudes. The direct consequence of this phenomenon is that PSV-induced directional scatter increasingly deviates from a Fisherian distribution (Fisher, 1953) with lower latitudes. This makes the commonly used standard Fisher statistical parameters (α_{95}, k) on directions inappropriate to describe PSV-induced scatter. A more realistic approach is to assume that the distribution of virtual geomagnetic poles (A_{95}, K) roughly follows a Fisherian distribution. The associated magnetic directions are a translation of this VGP distribution and are a function of site paleolatitude. In sediments, statistics describing a Fisherian distribution are thus better applied on the VGPs instead of the resulting magnetic directions. For within-site scatter that is described by Gaussian noise (e.g. as a result of measuring error within a recorded spot reading of the field, like a single lava flow or archaeomagnetic artifact), a Fisherian directional distribution (α_{95}, k) can be appropriately assumed.

In the literature, Fisher statistics are commonly applied to non-Fisherian distributions of paleomagnetic directions derived from sediments. Since the actual data in paleomagnetic research are seldom published or included in databases, and commonly only site mean directions are given, most published sedimentary paleomagnetic data include statistical parameters of direction distributions (α_{95}, k) that are unrepresentative of the dataset (Deenen et al., 2011). For this reason, Paleomagnetism.org provides Fisherian statistical parameters calculated for VGPs (A95, K) including separate errors for the declination (ΔD_x) and inclination (ΔI_x) after Butler (1992) for the associated directions. The module also

provides the Fisher parameters for directions (α_{95}, k) for sites where Fisherian directional distributions are appropriate.

The Geomagnetic Directions module (Fig. A5) illustrates a table containing Fisher parameters for directions and virtual geomagnetic poles after the selected cutoff has been applied. Directions and VGPs that are accepted or rejected by the cutoff are shown as blue and red dots respectively. The module generates two equal area projections (Fig. 3) showing directional data (left) and the associated relative virtual geomagnetic poles (right) with the average VGP rotated to the North Pole, to facilitate viewing the shape of the VGP distribution. Data can be viewed in either geographic or tectonic coordinates if a bedding orientation has been specified in the input. The illustrated blue-shaded confidence "parachute" (ΔD_x) is calculated from A95 and is a function of paleolatitude λ. This error represents the projected declination error on the horizontal plane (Butler, 1992). The red confidence envelope for the ChRM directions can be chosen as (i) the recommended projected Fisher (A95) cone of confidence from the VGPs distribution, (ii) the Fisher (α_{95}) circular cone of confidence for directions, or (iii) the Kent ellipse (Kent, 1982) that is an elliptical analog of the circular Fisher cone of confidence for non-uniformly distributed directions. The Kent ellipse describes a mathematical fit of the data and has no physical background; it is an ellipse that lies in the plane orthogonal to the mean direction and has the major and minor semi-axes in the direction of most and least scatter respectively (Kent, 1982; Tauxe et al., 2010). We provide the A95$_{min}$ and A95$_{max}$ as N-dependent parameters that quantify the minimum and maximum amount of dispersion for a distribution that can in principle be expected from paleosecular variation alone (Deenen et al., 2011). If A95 is lower than A95$_{min}$, PSV is not sufficiently recorded in the samples, and the data set describes for example a spot-reading of the geomagnetic field or remagnetization, and is in that case not representative of regional tectonics. If A95 exceeds A95$_{max}$, additional sources of scatter are expected besides just PSV, for example because of differential rotation or the NRM acquisition mechanism. These parameters are therefore especially important for rotational studies.

Multiple sites can be selected at once and all individual magnetic directions from these sites will be compiled to a temporary site, subjected to a new cut-off with new statistical parameters

describing the compiled distribution. This compiled site can be saved under a new name and added to the application; the user can choose to accept all directions from the combined sites, or to exclude the points rejected by the cutoff. Reversed directions can also be converted to a normal polarity.

3.2. Mean directions module

The mean directions module (Fig. A6) allows users to select multiple sites, and provides the mean directions and statistical parameters per individual site. The module illustrates the mean directions and confidence envelopes for all selected sites in geographic and tectonic coordinates. A table containing the full statistical parameters for all selected sites can be exported. Clicking the site names below the equal area plots provides a toggle to make the site mean visible for better readability in complicated overview plots.

3.3. Map overview and apparent polar wander path module

If site meta-data (e.g. location and age) are specified in the data input or advanced options tab, mean declinations can be illustrated in the application on a Google Maps overview (Figs. 4, and A7). The illustrated data are taken from Advokaat et al. (2014) with Triassic-Eocene sites colored in purple, and Miocene sites colored in orange. A directional marker with respective confidence "parachute" is indicated as visible marker constructed from the mean declination and uncertainty (ΔD_x). Site marker colors can be changed by the user to their preference by clicking the parachute. For any location, directions and virtual geomagnetic poles with confidence limits can be plotted together with the calculated declinations, inclinations, paleolatitudes, and apparent polar wander paths (Figs. 5 and A8) for a selection of the main plates (Africa, Arabia, Australia, Caribbean, China Blocks and Amuria; East Antarctica, Eurasia, Greenland, Iberia, India, Madagascar, North

America, Pacific, and South America). Three widely used global apparent polar wander paths (GAPWaPs) are included in our application. The default option is the GAPWaP of (Torsvik et al., 2012), from 320 Ma to present. The alternative options comprise Besse and Courtillot (2002), running from 200 Ma to present, and Kent and Irving (2010), running from 230 Ma to 50 Ma. These standard paths are rotated into the coordinates of each plate using the procedure used for Paleolatitude.org (van Hinsbergen et al., 2015). Lastly, a custom APWP can be added by the user for plates or ages not available by default in the application.

3.4. Common true mean direction (reversal test) module

The common true mean direction module (Fig. A9) assesses whether a given set of (antipodal) directions of two sites are statistically indistinguishable or not. If applied to two data populations of opposite magnetic polarity, this test becomes a reversal test. The CTMD test available on Paleomagnetism.org completes a Monte Carlo simulation to find a set of 2500 Watson parameters (Watson, 1983) for two distributions ($N1$, $\kappa1$), ($N2$, $\kappa2$). Per definition, these distributions are sampled around an identical mean direction and inherently share a common true mean direction. The critical Watson parameter is taken at the 95th percentile from the low-to-high sorted list of 2500 Watson parameters. From this critical Watson parameter, a critical angle is calculated that determines the upper limit for the angle between the two site means that may exist purely from random sampling of the distributions.

If the angle between the mean directions falls below the critical angle, the distributions share a common true mean and the quality of the simulation will be classified by A, B, C, or I in order of decreasing quality (see McFadden and McElhinny, 1990). Simulations where the angle between the mean directions exceeds the critical angle are marked by N and do not share a common true mean direction at the specified confidence level (Fig. 6a).

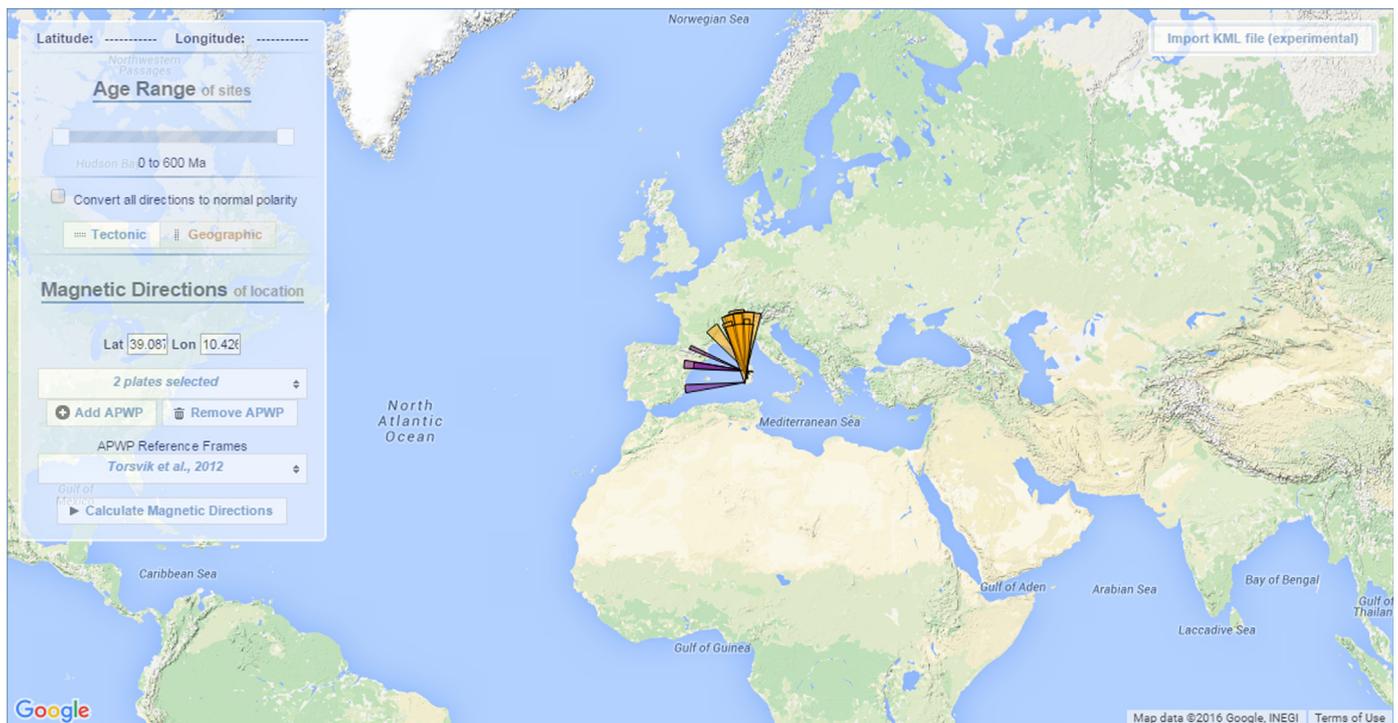The reversal or CTMD test by McFadden and McElhinny (1990)

Fig. 4. Map Module – Google Maps overview of Cretaceous – Eocene (purple) and Miocene (orange sites) showing the mean direction with confidence "parachutes" ΔD_x as calculated from A95. Site marker color can be changed by clicking the respective marker. The menu on the left allows for filtering of certain sites by age. This menu also calculates directions at a given site location for multiple standard APWPs for large continent-bearing plates. (For interpretation of the references to color in this figure legend, the reader is referred to the web version of this article.)
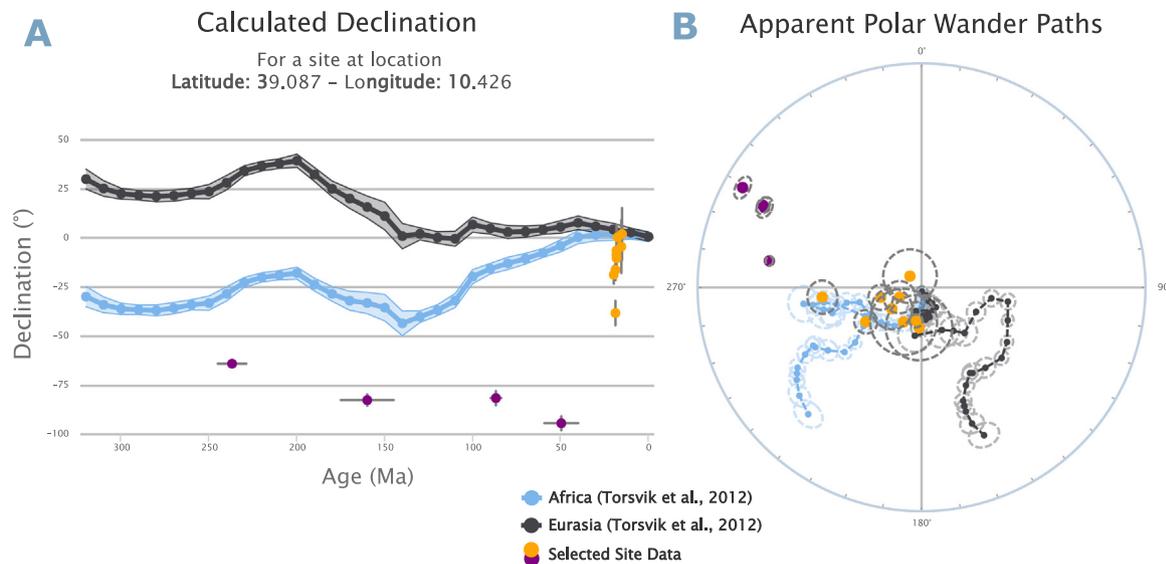
Fig. 5. Expected Directions and APWPs – (a) Graph showing the calculated declination for the indicated location (following the methodology of van Hinsbergen et al., 2015) with confidence limits for the African and European plate. The declination and confidence limit of all sites selected in the module are also visualized, granted that site location and age is specified. (b) Equal area projection showing apparent polar wander paths with A95 confidence limits for Africa and Europe from 320 to 0 Ma including the VGP positions of selected sites.

is often performed on directions, but we provide (as a default and recommended option) to perform the simulation on VGP distributions. The difference between the simulations comes from the assumption that not k (directional dispersion) but K (VGP dispersion) better approximates κ. We remark that the angle between two mean virtual geomagnetic poles is not equivalent to the angle between the associated directions, and that $R_{vgp} \neq R_{dir}$. We recommend this approach because geomagnetic directions at low latitudes often do not follow a Fisherian distribution while VGPs more realistically do.

Multiple sites can be tested simultaneously and a grid is displayed showing all possible permutations of the selected sites. When clicking one of the matrix tiles (Fig. A9), a non-parametric coordinate bootstrap is performed following the approach described by (Tauxe et al., 2010). This bootstrap calculates 5000 mean directions for the two sites and plots Cartesian coordinates with bootstrapped 95% confidence interval. The mean directions are translated to normal polarity if the angle between the directions exceeds 90°. This way, sets of directions on opposite sides of the equator are compared as is, and reversed and normal directions are converted to the same polarity. The result (Fig. 6b) shows bootstrapped (x, y, z) coordinates for both sites as a cumulative distribution function. If the confidence intervals for each coordinate overlap, the associated directions are statistically indistinguishable and the sites share a common true mean direction at 95% confidence level.

Comparison between sites can be done in geographic or tectonic coordinates, provided that bedding orientation has been specified by the user in the data input window.

3.5. Foldtest module

A foldtest aims to establish whether a magnetic vector was acquired prior to, during, or after folding. The foldtest module (Fig. A10) on Paleomagnetism.org follows the eigenvector approach of Tauxe and Watson (1994) and calculates the maximum eigenvalue of the orientation matrix of the data set for every percentage in the specified unfolding range (normally -50% to 150%). The maximum eigenvalue over this range is assumed to represent the largest degree of clustering for this site and the associated unfolding percentage is recorded. This procedure is repeated for the

selected amount of non-parametric bootstraps on N random selections of directions from the dataset. For each bootstrap, the unfolding percentage that yields the highest eigenvalue is recorded and shown as a cumulative distribution function (Fig. 7). The 95% confidence interval (shaded blue area) is determined by discarding the lower and upper 2.5% of sorted unfolding percentages for all bootstraps.

The bold red line in Fig. 7 indicates the progressive unfolding of the non-bootstrapped data and can be clicked to view the data at the respective percentage of unfolding. The light-blue curves illustrate the 25 first bootstraps.

3.6. Inclination shallowing (E/I) module

The inclination shallowing module (Fig. A11) aims to correct a dataset derived from compacted sedimentary rocks for the effects that compaction has on the inclination of the interpreted ChRM (Tauxe and Kent, 2004). For a given initial set of directions, the module calculates the elongation parameter (τ_2/τ_3) of the orientation matrix. For a given inclination, if the calculated elongation is lower than the expected elongation described by the TK03. GAD (Tauxe and Kent, 2004; Tauxe et al., 2008) field model, the flattening function of King (1955) is applied to unflatten the inclination by a small increment up to a maximum flattening factor of 0.2. This procedure is continued iteratively until an intersection with the TK03.GAD Polynomial is found. The procedure is completed for the actual data, and subsequently with 5000 non-parametric bootstraps. If no intersection with the polynomial is found for an individual bootstrap, it is discarded. A total number of 5000 attempts at bootstrapping are made. Fig. 8 shows an example of the simulation on data taken from Juárez et al. (1994), illustrating that all bootstraps found an intersection with the TK03. GAD polynomial and that the inclination may be corrected from roughly 42–53° with illustrated 95% confidence limits.

3.7. Statistics portal: advanced options

In the advanced options tab (Fig. A12), data can be exported to, and imported from the custom *.pmag* format that is the default extension for the statistics portal of the statistics portal. The option "edit site" allows a user to modify the site's data, location, age and
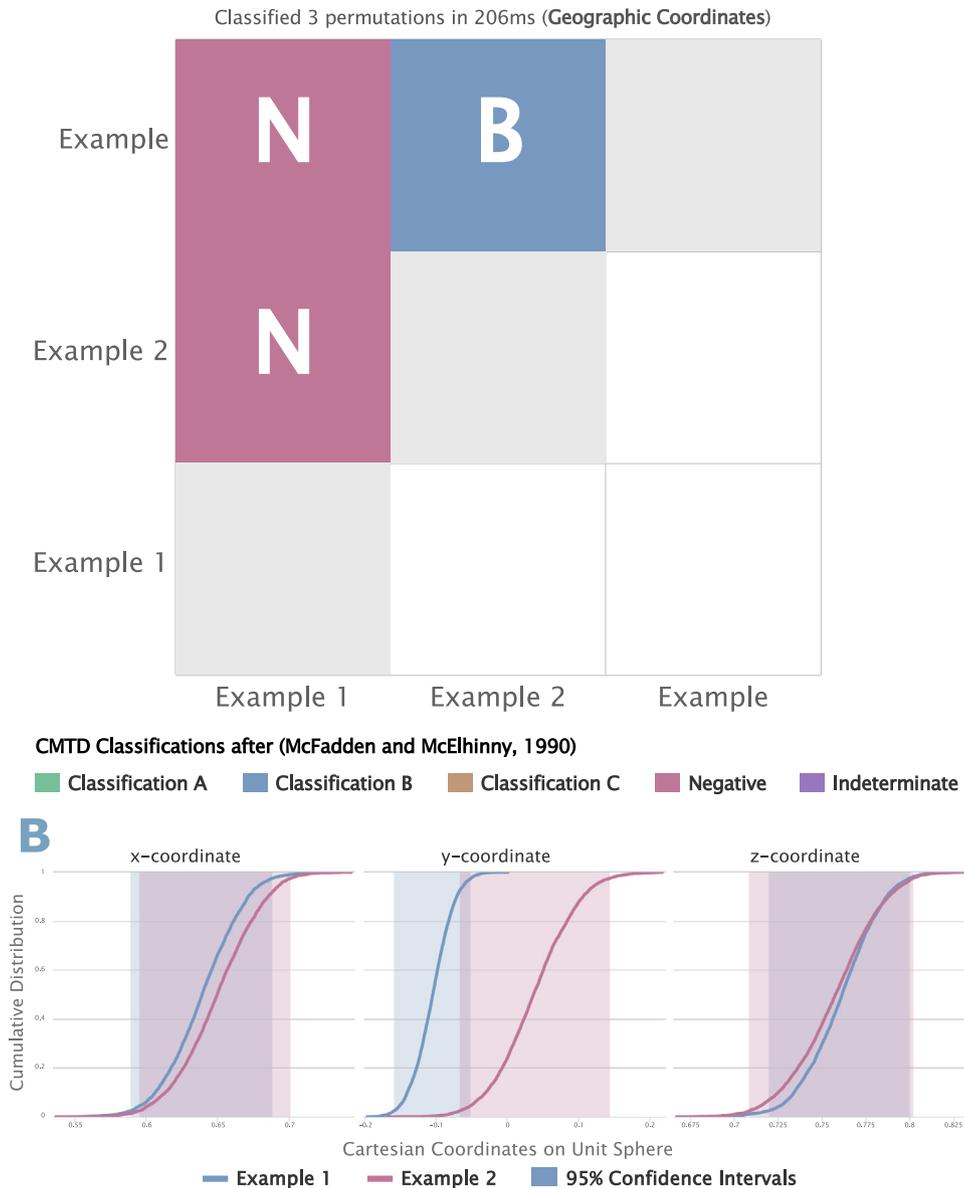
Fig. 6. CTMD Module – (a) Completed CTMD test showing a grid with three permutations for the three selected sites. The letters indicate the classification according to McFadden and McElhinny, 1990. The grid tiles are clickable and trigger a coordinate bootstrap as illustrated in the bottom figure. (b) Showing the cumulative distribution of the *x*, *y*, and *z* coordinates of the mean directions from 5000 non-parametric bootstraps of both sites. When the confidence levels of the two sites for all three individual coordinates overlap, they share a common true mean direction at 95% confidence.

age bounds (or alternatively the stage following GTS2012; Gradstein et al., 2012), the site description, and author. In addition, options can be chosen to change the default equal area projections into equal angle projections, and to color site mean directions individually rather than with one default color. Sites can be sorted in the select menu by name, age, or randomly. It is possible to reset the statistics portal, i.e. to remove all cached data stored locally within a browser with the reset button at the bottom of the page.

4. Miscellaneous portal

4.1. NTR analysis

The Net Tectonic Rotation (NTR) Analysis restores an orientation of a body (normally, a dyke) to a paleo-vertical (Fig. A13). The

analysis was originally developed by (Morris et al., 1998). We follow the methodology described by (Morris et al., 1998), but changed the errors assigned to paleomagnetic and reference directions from α_{95} to ΔD_x and ΔI_x after (Butler, 1992; Deenen et al., 2011). The algorithm is performed on directions and attempts to rotate (i) the pole to a dyke (with an α_{95} cone of confidence) to the horizontal plane while at the same time rotating (ii) the measured magnetization vector (with a ΔD_x and ΔI_x) to (iii) a reference magnetic direction (Fig. 8). This reference direction represents the expected paleomagnetic direction at the time of formation of the dyke. The declination of this reference direction is 0 or 180 for normal or reversed polarity, respectively, with no error (i.e., assuming the GAD hypothesis). The inclination is a function of the paleolatitude of the formation of the dykes, which may be predicted by e.g., an apparent polar wander path (in ΔI_x). This approach yields two solutions for the initial dyke orientation, per
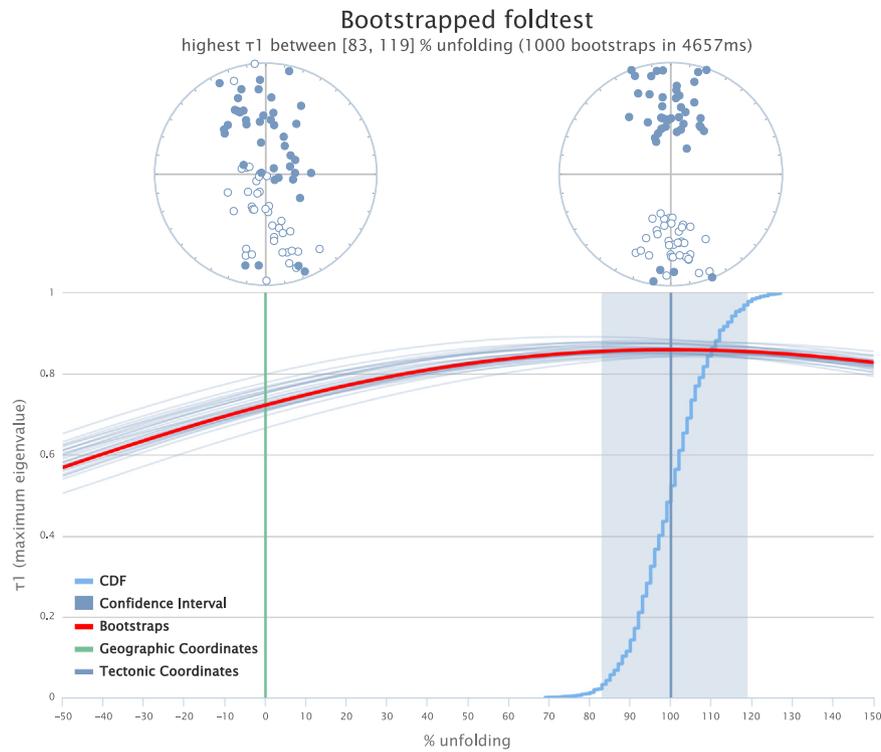
Fig. 7. Foldtest Module – Foldtest result illustrating geomagnetic directions in geographic and tectonic coordinates at the top. The unfolded data is represented by the bold red curve and the first 25 bootstraps by light-blue lines. The maximum eigenvalue at a particular unfolding percentage is recorded and shown as a CDF with 95% confidence limits for 1000 bootstraps. Data is taken from the "foldtest_example.dat" provided by the PmagPy library (see https://earthref.org/PmagPy/cookbook/#x1-1000005.2.44). (For interpretation of the references to color in this figure legend, the reader is referred to the web version of this article.)
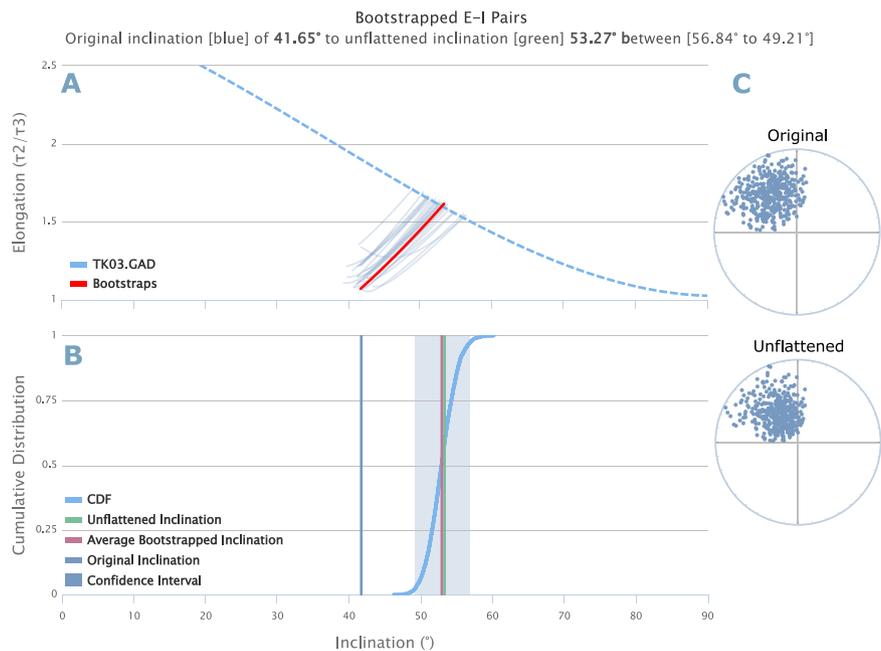

Fig. 8. Inclination Shallowing Module – showing (a) the TK03.GAD fitted polynomial (after Tauxe et al., 2008) and the progressive unflattening of the actual data in the bold red curve, including the first 25 bootstraps in light blue. (b) The inclination of the intersection with the polynomial is recorded and shown as a CDF with 95% confidence limits for 5000 bootstraps. (c) The geomagnetic directions before and after the correction. Data for the simulation was taken from Juárez et al. (1994) (P-component). (For interpretation of the references to color in this figure legend, the reader is referred to the web version of this article.)

polarity (Fig. 9) (see Morris et al., 1998 for a detailed explanation of the procedure). The two solutions frequently predict very differently inclined-axis rotations, which may help the choice of the preferred solution using independent geological data. Included with the NTR solutions we provide the predicted great-circles that show the orientation of a paleo-horizontal after rotation over the

two NTR solutions. To qualitatively assess a non-parametric confidence interval around the NTR solution, the analysis can be iterated by taking permutations of points on the edges of the specified confidence envelopes for the three input vectors. This method yields a collection of 75 solutions representing an irregularly shaped confidence interval of the actual pair of solutions.
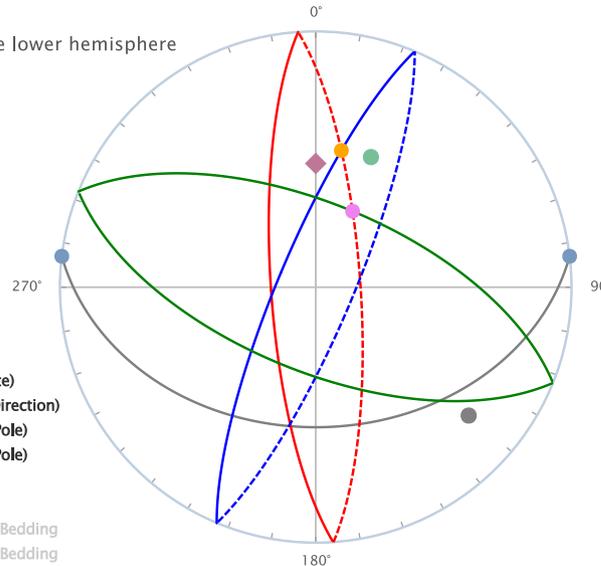
Fig. 9. NTR Module – An example illustrating three input vectors (reference pole, magnetization vector, and dyke pole). The intersection of a circle with radius β (angle between dyke pole and magnetization vector) around the reference pole with the horizontal determines a maximum of two points. From these intersections and the input reference pole, three bisector planes are calculated. The two requested rotation poles are located at the intersections of these bisectors. For a detailed explanation of the procedure we refer to the original authors (Morris et al., 1998).

The densities of the original pole to dyke are expressed in a rose diagrams for each solution (Fig. A13).

4.2. Oroclinal test module

This module includes an oroclinal test (Fig. A14), which as a formal test with statistical error bounds has not been published before. An orocline is a thrust belt or orogen that is curved in map – view due to it having been bent or buckled about a vertical axis of rotation (Carey, 1955). Two distinct types of oroclines are recognized: progressive and secondary (Johnston et al., 2013). The orocline test (or strike test; Eldredge et al., 1985; Schwartz and Vandervoo, 1983; Pastor-Galán et al., 2011) evaluates the relationship between variations in regional structural trend and the orientations of given geologic fabric elements (e.g., paleomagnetic declinations, fractures, cleavage, veins, lineations, etc.) through linear regression of bi-dimensional data. The expected slope in the oroclinal test ranges between 1 (linear relationship between declination and strike; secondary oroclines) and 0 (no relationship; primary arcs with no vertical-axis rotation). We provide a method to bootstrap the data within their error margins following a standard sampling method (homogenous throughout the error bounds) or Gaussian method (following a Box–Muller transform (Box and Muller, 1958)). From these simulations we calculate a bootstrapped 95% confidence interval using a total least squares linear regression. The resulting graph (Fig. 10a) shows the bi-dimensional data with specified uncertainties and the 95% bootstrapped confidence interval. The linear regression and confidence interval on this regression can be applied on any bi-dimensional data and is not limited as an application in the oroclinal test. We also provide the statistical approach of (Yonkee and Weil, 2010), a weighed least squares regression that weigh the individual site errors to obtain the best fit line. A variety of other statistical tools are implemented to help visualize the distribution of the data residuals to the regression (see Appendix Fig. A14).

Additionally, we have adapted the eigenvector approach fold test (Tauxe and Watson, 1994) to the oroclinal test by rotation around a vertical axis and recording the minimum circular variance with all inclinations implicitly set to 0. We can faithfully use circular statistics because by setting the inclination to zero we have reduced the clustering to a single dimension (i.e. the declinations lie between 0 and 360). The result (Fig. 10b) illustrates a similar diagram to the Paleomagnetism.org foldtest in addition to a rose diagram with the density of declinations for the clicked percentage of unfolding. For the dedicated publication to the software available in the module we refer to (Pastor-Galán et al., 2016).

5. Paleomagnetism.org availability, disclaimer, and license

The Paleomagnetism.org application can be reached and works under all modern browsers (e.g. Firefox, Internet Explorer, Chrome, and Safari). An offline version can be downloaded and used without an internet connection. The source-code is available on GitHub: https://github.com/Jollyfant/Paleomagnetism.org. Features that require an internet connection (e.g. figure exporting and the Google Maps overview) will not work in offline-mode.

All data processing is performed on the client side to respect the integrity of the data and users, with the exception of figure exporting. Data information for a session is stored locally within the 5MB allocated local storage feature within browsers. This data is automatically loaded to the application once the application is restarted. Clearing the browser's local storage in the advanced options tab will remove any stored information.

Paleomagnetism.org is an open-source initiative licensed under the GNU General Public License v3.0.

6. Conclusion

Paleomagnetism.org provides an open-source and multi-platform online environment to do convenient data analysis that promotes making data easily available to the paleomagnetic community. All diagrams in the application can be exported to high quality .png, .pdf, .svg formats by clicking the stacked marker at the top right of each figure. Our application offers a collection of tools for interpretation (e.g. principle component analysis
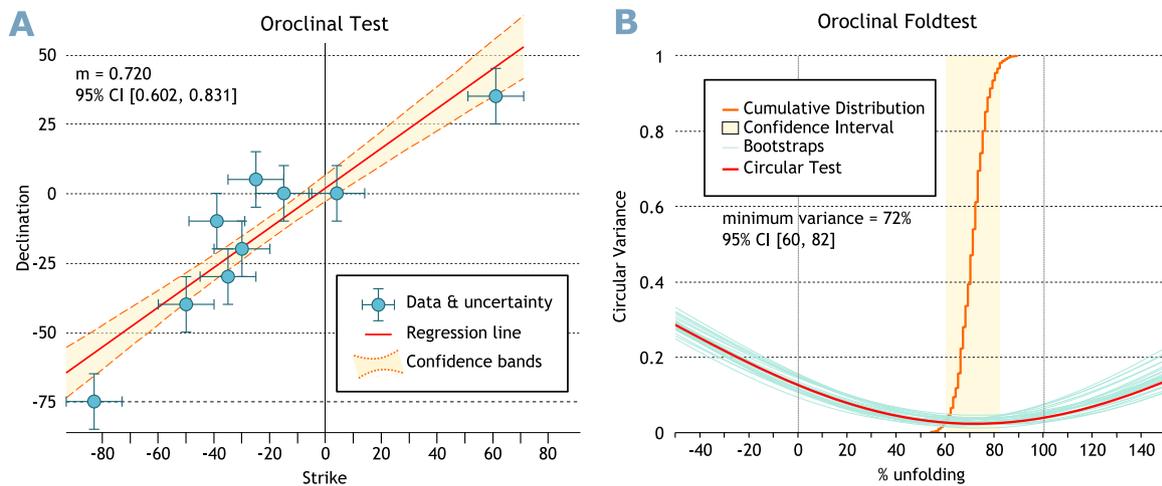
Fig. 10. Oroclinal Module – Showing (a) A standard oroclinal test using a linear regression for the data including bootstrapped confidence limits. Example data is taken from (Pastor-Galán et al., 2011). (b) An oroclinal foldtest illustrating the CDF of percentage of unfolding with the lower circular variance (i.e. best clustering). The bold red curve illustrates the procedure for the actual data, with the first 25 bootstraps indicated in light-blue. For details, we refer to the detailed standalone publication about this procedure (Pastor-Galán et al., 2016). (For interpretation of the references to color in this figure legend, the reader is referred to the web version of this article.)

including great circles solutions) and the statistical treatment (e.g. Fisher statistics, foldtest, reversal tests, inclination shallowing correction, predicted geomagnetic directions, and APWP visualization) useful for standard paleomagnetic analysis. It also includes miscellaneous tools for more specialized studies (e.g. oroclinal test, NTR analysis). The accessibility, coherency, and ease by which data can be interpreted, evaluated, visualized, and shared will make Paleomagnetism.org of interest to the paleomagnetic community.

Acknowledgments

Appendix A. Supplementary material

Supplementary data associated with this article can be found in the online version at http://dx.doi.org/10.1016/j.cageo.2016.05.007.

References

Advokaat, E.L., van Hinsbergen, D.J.J., Maffione, M., Langereis, C.G., Vissers, R.L.M., Cherchi, A., Schroeder, R., Madani, H., Columbu, S., 2014. Eocene rotation of Sardinia, and the paleogeography of the western Mediterranean region. Earth Planet. Sci. Lett. 401, 183–195.

Besse, J., Courtillot, V., 2002. Apparent and true polar wander and the geometry of the geomagnetic field over the last 200 Myr. J. Geophys. Res. 107, 2300, doi:10.1029–2000JB000050.

Biggin, A., van Hinsbergen, D.J.J., Langereis, C.G., Straathof, G.B., Deenen, M.H., 2008. Geomagnetic secular variation in the cretaceous normal superchron and in the Jurassic. Phys. Earth Planet. Inter. 169, 3–19.

Box, G., E., P., Muller, M., E., 1958. A note on the generation of random normal deviates. Ann. Math. Stat. 29 (2), 610–611.

Butler, R.F., 1992. Paleomagnetism. Wiley-Blackwell, United States.

Carey, S.W., 1955. The orocline concept in geotectonics. R. Soc. Tasmania Proc. 89.

Cox, A., 1970. Latitude dependence of the angular dispersion of the geomagnetic field. Geophys. J. Int. 20, 253–269.

Creer, K.M., 1962. The dispersion of the geomagnetic field due to secular variation and its determination for remote times from paleomagnetic data. J. Geophys. Res. 67, 3461–3476.

Deenen, M.H.L., Langereis, C.G., van Hinsbergen, D.J.J., Biggin, A.J., 2011. Geomagnetic secular variation and the statistics of palaeomagnetic directions. Geophys. J. Int. 186 (2), 509–520.

Eldredge, S., Bachtadse, V., Van Der Voo, R., 1985. Paleomagnetism and the orocline hypothesis. Tectonophysics 119, 153–179.

Gradstein, Felix M., Ogg, James G., Schmitz, Mark D., Ogg., Gabi M., 2012. The Geologic Time Scale. 2012. Elsevier, Oxford, U.K..

Fisher, R.A., 1953. Dispersion on a sphere. Proc. R. Soc. Lond. A217, 295–305.

Johnson, C.L., et al., 2008. Recent investigations of the 0–5 Ma geomagnetic field recorded by lava flows. Geochem. Geophys. Geosyst. 9 (4), Q04032, doi:10.1029.2007GC001696.

Johnston, S.T., Weil, A.B., Gutierrez-Alonso, G., 2013. Oroclines: thick and thin. Geol. Soc. Am. Bull. 125, 643–663.

Juárez, M.T., Osete, M.L., Meléndez, G., Langereis, C.G., Zijderveld, J.D.A., 1994. Oxfordian magnetostratigraphy of the Aguilón and Tosos sections (Iberian Range, Spain) and evidence of a pre-Oligocene overprint. Phys. Earth Planet. Inter. 85 (1), 195–211.

Kent, D.V., Irving, E., 2010. Influence of inclination error in sedimentary rocks on the Triassic and Jurassic apparent pole wander path for North America and implications for Cordilleran tectonics. J. Geophys. Res. 115 (B10), B10103, doi:10.1029–2009JB007205.

Kent, J.T., 1982. The Fisher-Bingham distribution on the sphere. J. R. Stat. Soc. B 44, 71–80.

King, R.F., 1955. The remanent magnetism of artificially deposited sediments. Mon. Not. R. Astron. Soc. 7, 115–134.

Kirschvink, J.L., 1980. The least-squares line and plane and the analysis of palaeomagnetic data. Geophys. J. R. Astrol. Soc. 62, 699–718.

McFadden, P.L., McElhinny, M.W., 1988. The combined analysis of remagnetisation circles and direct observations in paleomagnetism. Earth Planet. Sci. Lett. 87, 161–172.

McFadden, P.L., McElhinny, M.W., 1990. Classification of the reversal test in palaeomagnetism. Geophys. J. Int. 103, 725–729.

Morris, A., Anderson, M.W., Robertson, A.H.F., 1998. Multiple tectonic rotations and transform tectonism in an intraoceanic suture zone, SW Cyprus. Tectonophysics 299, 229–253.

Pastor-Galán, D., Gutiérrez-Alonso, G., Weil, A.B., 2011. Orocline timing through joint analysis: Insights from the Ibero-Armorican Arc. Tectonophysics 507, 31–46.

Pastor-Galán, D., Mulchrone K.F., Koymans, M.R., van Hinsbergen, D.J.J., Langereis, C. G., 2016, Total least squares orocline test: a robust method to quantify vertical axis rotation patterns in orogens, with examples from the Cantabrian and Aegean oroclines (In preparation).

Schwartz, S.Y., Vandervoo, R., 1983. Paleomagnetic evaluation of the orocline hypothesis in the Central and Southern Appalachians. Geophys. Res. Lett. 10, 505–508.

Tauxe, L., Watson, G.S., 1994. The fold test: an eigen analysis approach. Earth Planet. Sci. Lett. 122, 331–341.

Tauxe, L., Kent, D.V., 2004. A simplified statistical model for the geomagnetic field and the detection of shallow bias in paleomagnetic inclinations: was the ancient magnetic field dipolar? In: Channell, J., Kent, D., Lowrie, W., Meert, J. (Eds.), Timescales of the Paleomagnetic Field 145. American Geophysical Union, Washington, D.C, pp. 101–116.

Tauxe, L., Kodama, K.P., Kent, D.V., 2008. Testing corrections for paleomagnetic inclination error in sedimentary rocks: a comparative approach. Phys. Earth Planet. Inter. 169, 152–165.

Tauxe, L., Butler, R.F., Van der Voo, R., Banerjee, S.K., 2010. Essentials of Paleomagnetism. University of California Press, California, ISBN: 9780520260313.

Tauxe, L, Shaar, R., Jonestrask, L, Swanson-Hysell, N.L, Minnett, R., Koppers, A.A.P., Constable, C.G., Jarboe, N., Gaastra, K., Fairchild, L., 2016. PmagPy: Software package for paleomagnetic data analysis and a bridge to the Magnetics Information Consortium (MagIC) Database. Geochem. Geophys. Geosyst. http://dx.doi.org/10.1002/2016GC006307.

Torsvik, T.H., et al., 2012. Phanerozoic polar wander, palaeogeography and dynamics. Earth Sci. Rev. 114, 325–368.

van Hinsbergen, D.J.J., de Groot, L.V., van Schaik, S.J., Spakman, W., Bijl, P.K., Sluijs, A., Langereis, C.G., Brinkhuis, H., 2015. A paleolatitude calculator for paleoclimate studies. PLoS ONE 10, e0126946–21. http://dx.doi.org/10.1371/journal.pone.0126946.

Vandamme, D., 1994. A new method to determine paleosecular variation. Phys. Earth Planet. Inter. 85, 131–142.

Watson, G., 1983. Large sample theory of the Langevin distributions. J. Stat. Plann. Inference 8, 245–256.

Yonkee, A., Weil, A.B., 2010. Reconstructing the kinematic evolution of curved mountain belts: Internal strain patterns in the Wyoming salient, Sevier thrust belt, U.S.A. Geol. Soc. Am. Bull. 122, 24–49.

Zijderveld, J.D.A., 1967. A.C. demagnetization of rocks: analysis of results. In: Collinson, D.W., Creer, K.M., Runcorn, S.K. (Eds.), Methods in Palaeomagnetism. Elsevier, Amsterdam, New York, pp. 254–286.